https://doi.org/10.2352/ISSN.2470-1173.2019.13.COIMG-147

Edge-Preserving Total Variation Regularization for Dual-Energy CT Images

Sandamali Devadithya, David Castañón; Boston University; Boston, MA/U.S.A.

Abstract

Dual-energy computed tomography (CT) offers the potential to recognize material properties by decomposing sinograms into Compton and photoelectric bases and subsequently reconstructing the Compton and photoelectric images. However, the presence of high density materials such as metal can distort the reconstructed images, leading to inaccurate material characterization. In this paper, we present a reconstruction technique to reduce noise and metal artifacts in dual-energy CT images by exploiting (1) statistical correlation between measurements and decomposed sinograms, (2) intra-image correlation between decomposed images, and (3) inter-image sparsity. The algorithm is based on minimizing weighted least squares with edge-preserving total variation regularization and is solved using split-Bregman iterative techniques. Using experimental data acquired from a commercial scanner, we demonstrate that the proposed algorithm significantly reduces noise and metal artifacts compared to the baseline approaches of filtered back projection and competing iterative reconstructions algorithms.

Introduction

Computed tomography (CT) imaging with X-rays is a non destructive way of imaging volumes, with broad applications in medical, industrial and security. When an X-ray beam travels through an object, the beam gets attenuated based on the object material properties, characterized by the energy-dependent linear attenuation coefficient (LAC). The object can be identified by reconstructing the LAC at different spatial locations, which is estimated from the photon intensities measured at multiple detectors using CT reconstruction algorithms.

In conventional CT algorithms, the reconstruction is based on a monochromatic approximation of the photons generated by an X-ray source. However, common X-ray sources generate photons at multiple energies, with spectral distribution corresponding to a Bremsstrahlung spectrum. Since detectors are either energy integrating detectors or photon counting detectors, they measure an average statistic over all the photons received. Thus, the CT reconstruction estimates an average linear attenuation coefficient. This leads to beam hardening artifacts [1] and difficulty in recognizing different materials. As an alternative, dual-energy X-ray projection systems were developed, where the transmission properties of two different source energy spectra are measured at each detector. In such systems, one can compute linear attenuation coefficients at two different average energies, which provides a better characterization of the energy-dependent LAC properties of materials and leads to improved material recognition. However, the reconstructed individual average attenuation images still suffer from significant artifacts due to the monochromatic approximations and the high attenuation caused by the presence of dense materials.

In order to account for the polychromatic nature of the X-ray sources and alleviate the beam-hardening artifacts, a common approach used in dual-energy reconstruction is to expand the energy-dependent linear attenuation coefficients of materials in terms of two basis functions, and reconstruct the coefficients of these basis functions at different spatial locations [2, 3]. A common set of basis functions used are photoelectric absorption and Compton scatter functions, corresponding to two of the primary energy-dependent physical processes that lead to the loss of photons on the path from source to detector. Starting from the measured values at each detector for the two spectral excitations, one can exploit knowledge of the source-detector spectral characteristics to estimate equivalent Compton and photoelectric measurements at each detector. The resulting photoelectric and Compton sinograms are subsequently processed by CT reconstruction algorithms such as filtered back-projection (FBP) [2, 4] to generate volumetric Compton and photoelectric coefficient images. However, the presence of metal or other dense materials significantly distorts the reconstructed images, particularly the photoelectric image, as the photoelectric absorption rate at lower energies is significantly higher in metal, and is difficult to estimate given the detector measurements.

In the conventional single-energy spectrum setting, common approaches to correct metal artifacts are based on interpolating the metal regions of the sinogram projection data or on post-processing the corrupted images [5, 6]. However, there has been little work focusing on alleviating metal artifacts in dual-energy imaging using basis decompositions.

One interesting approach for enhancing the quality of dual-energy images is to exploit the structure similarity between the Compton and photoelectric images. In [7], the authors proposed an iterative model-based joint inversion framework to estimate both photoelectric and Compton coefficients directly from the dual-energy measurements. They proposed to stabilize the photoelectric image using patch-based regularization based on the previous iteration's Compton image estimation. However, metal induced streaks were clearly visible in final Compton and photoelectric images estimated, and the proposed method is computationally inefficient. In [8], the authors proposed a joint reconstruction method based on the Mumford-Shah functional to jointly estimate the Compton image, the photoelectric image, and the image boundary field from the decomposed sinograms with the use of Tiknohov regularization terms. This method is referred to as structure preserving dual energy (SPDE) inversion method. This method requires the estimation of the third volumetric field (the boundary field), and shows limited success in reducing the metal artifacts, as the estimation depends on the Compton and photoelectric sinogram decompositions.

In this paper we present a model-based iterative algorithm to reduce the effects of noise and metal artifacts in dual-energy CT images, based on edge-preserving total variation (EPTV) regularization. In [9], the authors proposed an iterative CT reconstruction algorithm with EPTV regularization. The idea behind the EPTV is to perform smoothing only on non-edge parts of the image and it is realized by introducing a penalty weight to the original TV norm. We extend this idea for dual-energy CT reconstructions, exploiting the fact the edges are common for both Compton and photoelectric images. Edges are identified using an initial reconstruction of the high energy image, avoiding errors introduced in the decompositions into photoelectric and Compton sinograms. Once the edges are found, we reconstruct the Compton and the photoelectric images using EPTV regularization such that the edges in both images are not smoothed.

Even though the noise and metal artifacts in Compton images can be mitigated with EPTV regularization, the metal artifacts in photoelectric images cannot be corrected only by EPTV. When data is highly corrupted, the decomposition into photoelectric and Compton bases is ill-conditioned, and the resulting estimated inverse error covariance is nearly singular in the direction of the photoelectric coefficient. To account for this, we use the inverse photoelectric covariance to down-weight the photoelectric coefficient estimates in the photoelectric sinograms. Down-weighting the photoelectric sinogram was also proposed in the SPDE inversion method [8]. However, the weighting matrix they proposed was based on the high-energy sinogram, and had no direct relationship to the photoelectric sinogram.

We apply split-Bregman techniques [10] to solve the final optimization problem of minimizing weighted least squares with edge-preserving total variation regularization. We provide experimental validation with dual-energy data acquired from a commercial scanner with images that contain significant metal scatter. We show that the proposed method is superior over the state-of-practice filtered back projection method used in the commercial scanner as well as TV iterative reconstruction techniques and the SPDE inversion method.

The rest of the paper is organized as follows: we give an overview of dual-energy X-ray image formation, followed by a detailed description of the proposed algorithm. Next we present our experiments and conclude with a discussion of results and some ideas for future work.

Measurement Model

Dual-energy CT systems capture two measurements of the scene acquired with two different X-ray spectral distributions. According to the Beer-Lambert law the expected photon counts along X-ray path L_j is modeled as

$$I_i(j) = \int I_0 w_i(E) e^{-\int_{L_j} \mu(r,E) dl} dE \tag{1}$$

Here $i = 1,2$ denotes the system spectrum index, while $j = 1,2,..M$ denotes the detector index, where the total number of detectors are M. The rest of the terms are: E is the energy level, r is the spatial location, $\mu(r,E)$ is the linear attenuation coefficient (LAC) at energy E and position r along the X-ray path L_j, $w_i(E)$ is the i^{th} normalized spectrum at energy E and includes the energy-dependent source strength and detector sensitivity, and I_0 is the source intensity. When dealing with photon counting detectors, the actual received counts at detector j, $Z_i(j)$, divided by the counts obtained from a clear path from the X-ray source to the detector, can be modelled as a Poisson process with the mean given by (1) , ignoring the effects of background radiation. We use as measurements the negative log of the normalized intensity or photon counts, referred to as sinograms. Let $s_i(j)$ denote the i^{th} energy sinogram at detector j, defined as

$$s_i(j) = -\ln(\frac{Z_i(j)}{Z_0(j)}) \tag{2}$$

where $Z_0(j)$ are the expected photon counts from a direct path with no attenuation on projection L_j. Within the energy range of medical and security CT imaging (20 to 150 keV), the main physical processes that lead to photon loss in the ray path from source to detector attenuation are Compton scatter and photoelectric absorption. Thus, the energy-dependent LAC of many materials can be approximated in terms of Compton scatter and photoelectric absorption basis functions, as [2]

$$\mu(r,E) = x_c(r) f_c(E) + x_p(r) f_p(E) \tag{3}$$

where $x_c(r)$ and $x_p(r)$ are the Compton and photoelectric coefficients of the material at spatial location r respectively, and $f_c(E)$ is the energy-dependent Compton scatter basis functions which is approximated by the Klein-Nishina function [2]

$$f_c(\alpha) = \frac{1+\alpha}{\alpha^2}\big(\frac{2(1+\alpha)}{1+2\alpha} - \frac{1}{\alpha}\ln(1+2\alpha)\big) + \frac{1}{2\alpha}\ln(1+2\alpha) - \frac{1+3\alpha}{(1+2\alpha)^2}$$

and $f_p(E)$ is the photoelectric absorption basis function, approximated by

$$f_p(E) = \frac{1}{E^3}.$$

Using the basis decomposition in (3), the expected value of normalized counts in (1) can be written as

$$I_i(j) = \int w_i(E) e^{-(\int_{L_j} x_c(r) f_c(E) + x_p(r) f_p(E) dl)} dE \tag{4}$$

The Compton and photoelectric projections at each detector are defined as $y_c(j) = \int_{L_j} x_c(r) dl$ and $y_p(j) = \int_{L_j} x_p(r) dl$ respectively. The first step in dual-energy basis material reconstruction is to decompose the high and low energy sinograms $s_1(j), s_2(j)$ into Compton and photoelectric sinograms $y_c(j), y_p(j)$. We do this using a nonlinear least squares minimization, where we minimize

$$\min_{y_c, y_p} \sum_{i=1}^{2} Z_i(j)(s_i(j) + \ln \int w_i(E) e^{-y_c f_c(E) - y_p f_p(E)} dE)^2 \tag{5}$$

Here we use the measured counts as an approximation to the inverse variance of the measurements, as in [11]. In this paper, we generate the estimates $y_c(j), y_p(j)$ by solving the above minimization problem (5) using a non-linear Gauss-Newton method [12]. Thereafter, the sinograms and the respective coefficients can be linearly modeled using the forward projection matrix $\mathbf{A}$ as,

$$\mathbf{y}_c = \mathbf{A}\mathbf{x}_c \tag{6}$$

$$\mathbf{y}_p = \mathbf{A}\mathbf{x}_p \tag{7}$$

The most widely used approach for reconstructing $\mathbf{x}_c$ and $\mathbf{x}_p$ is to apply filtered back-projection (FBP) on (6) and (7) respectively. In the presence of metal in the image, this can create significant distortions, as we will show in our examples.

Proposed Method

In this section we discuss the algorithm proposed to reduce the noise and metal artifacts in dual-energy CT images. The framework is a model-based iterative reconstruction algorithm to minimize weighted least squares with edge-preserving total variation regularization (EPTV). We exploit (1) statistical correlation between measurements and decomposed sinograms, (2) intra-image correlation between decomposed images, and (3) inter-image sparsity. The general solution is as,

$$\hat{\mathbf{x}}_c = \underset{\mathbf{x}_c \geq 0}{\operatorname{argmin}} \frac{1}{2}||\mathbf{y}_c - \mathbf{A}\mathbf{x}_c||^2_{W_{yc}} + \tau_c R(\mathbf{x}_c) \tag{8}$$

$$\hat{\mathbf{x}}_p = \underset{\mathbf{x}_p \geq 0}{\operatorname{argmin}} \frac{1}{2}||\mathbf{y}_p - \mathbf{A}\mathbf{x}_p||^2_{W_{yp}} + \tau_p R(\mathbf{x}_p) \tag{9}$$

for Compton and photoelectric coefficients respectively. Here $R(\mathbf{x}_c)$ and $R(\mathbf{x}_p)$ are the regularization terms, τ_c and τ_p are the regularization parameters, and W_{yc}, W_{yp} are weighting terms for the data fidelity. In the following subsections, we describe how the parameters for each problem are selected.

Covariance Matrices of Basis Sinograms

Since the proposed solution is built on the estimated basis sinograms $\mathbf{y}_c$ and $\mathbf{y}_p$, we first consider the errors associated with estimating these quantities. Using approximations based on non-linear estimation, the inverse covariance matrices of the estimated parameters $y_c(j), y_p(j)$ at detector j associated with a maximum likelihood estimator is given by

$$P = \mathbf{J}^T \begin{bmatrix} Z_1(j) & 0 \\ 0 & Z_2(j) \end{bmatrix} \mathbf{J} \tag{10}$$

where $\mathbf{J}$ is the Jacobian matrix of the transformation

$$\begin{bmatrix} f_1(y_c, y_p) \\ f_2(y_c, y_p) \end{bmatrix} = \begin{bmatrix} -\ln \int w_1(E) e^{-y_c f_c(E) - y_p f_p(E)} dE \\ -\ln \int w_2(E) e^{-y_c f_c(E) - y_p f_p(E)} dE \end{bmatrix}$$

We found that in the presence of metal, the inverse covariance matrices are nearly singular with high condition numbers, as shown in Fig. 3 in the results section below. We also noted that the direction of the minimum eigenvalue corresponds closely to the photoelectric coefficient, indicating that the estimates of this coefficient have very high variance. This agrees with the fact that the higher attenuation in dense materials such as metal prevents most of the low energy photons from reaching the detector, and make it difficult to reliably estimate the photoelectric coefficients at lower energies, where that effect is best observed . To account for this phenomenon, we apply explicit weighting $W_{yp}(j)$ to each detector j in the photoelectric sinogram, with weights defined as the (2,2) element of the matrix in (10) for each j. This results in the diagonal weighting matrix W_{yp} used in (9). We can apply a similar process to obtain a weight W_{yc} for the Compton sinograms in (8). However, Compton values are much better behaved, and additional weighting will not make much difference in the reconstruction quality.

Edge-Preserving Total Variation Regularization

The idea behind the EPTV regularization is to perform smoothing only on non-edge parts of the image. We accomplish this as in [9], by penalty weight modifying the total variation (TV) norm in the regularization. We use the TV norm to obtain sharp smoothing, as opposed to the L2 regularization norm used in [8]. Specifically, we use the anisotropic TV [10], as

$$R(\mathbf{x}) = ||\mathbf{D}_h\mathbf{x}||_1 + ||\mathbf{D}_v\mathbf{x}||_1 \tag{11}$$

where $\mathbf{D}_h$ and $\mathbf{D}_v$ are horizontal and vertical gradient operators approximated by the finite differences. To avoid blurring the edges, we add a penalty weight, so the regularization term becomes,

$$R(\mathbf{x}) = ||\mathbf{W}_h\mathbf{D}_h\mathbf{x}||_1 + ||\mathbf{W}_v\mathbf{D}_v\mathbf{x}||_1 \tag{12}$$

where $\mathbf{W}_h$ and $\mathbf{W}_v$ are diagonal matrices with weights for horizontal and vertical directions respectively.

In order to assign the penalty weights we first need to locate the edges. Since when doing basis decomposition there is a possibility of losing information and introducing additional errors, we identify the edges based on a reconstruction of the high-energy image, which has higher signal-to-noise ratio compared with the low energy image, and the higher energy photons are more likely to reach the detectors. We reconstruct the high-energy image via an iterative algorithm, minimizing weighted least squares with TV regularization as follows.

$$\hat{\mathbf{x}}_{high} = \underset{\mathbf{x}_{high} \geq 0}{\operatorname{argmin}} \frac{1}{2}||\mathbf{s}_{high} - \mathbf{A}\mathbf{x}_{high}||^2_{\tilde{W}} + \tau||\mathbf{D}_h\mathbf{x}_{high}||_1 + \tau||\mathbf{D}_v\mathbf{x}_{high}||_1 \tag{13}$$

with $W = diag(\mathbf{Z}_{high})$. Once we reconstruct the high-energy image the penalty weights are assigned as,

$$\mathbf{w}_v = \exp(-(|\mathbf{D}_v\mathbf{x}_{high}|)/\sigma) \tag{14}$$

$$\mathbf{w}_h = \exp(-(|\mathbf{D}_h\mathbf{x}_{high}|)/\sigma) \tag{15}$$

where σ is the controlling parameter. Once the penalty weights are assigned, the optimization problems in (8) and (9) are defined.

Optimization Approach

Based on the above discussion, the final solutions for Compton and photoelectric coefficients are obtained from the following optimization problems.

$$\hat{\mathbf{x}}_c = \underset{\mathbf{x}_c \geq 0}{\operatorname{argmin}} \frac{1}{2}||\mathbf{y}_c - \mathbf{A}\mathbf{x}_c||^2_2 + \tau_c||\mathbf{W}_h\mathbf{D}_h\mathbf{x}_c||_1 + \tau_c||\mathbf{W}_v\mathbf{D}_v\mathbf{x}_c||_1 \tag{16}$$

$$\hat{\mathbf{x}}_p = \underset{\mathbf{x}_p \geq 0}{\operatorname{argmin}} \frac{1}{2}||\mathbf{y}_p - \mathbf{A}\mathbf{x}_p||^2_{\mathbf{W}_{yp}} + \tau_p||\mathbf{W}_h\mathbf{D}_h\mathbf{x}_p||_1 + \tau_p||\mathbf{W}_v\mathbf{D}_v\mathbf{x}_p||_1 \tag{17}$$

Problems (16) and (17), as well as (13) are convex but non-differentiable functions and hence cannot be solved in closed form solutions. For computational efficacy and numerical stability we chose to use split-Bregman techniques [10] to solve each of the

problems. Here we describe the problem (17) as an example, and the other sub-problems can be similarly implemented. To enable Bregman splitting we introduce two auxiliary variables $\mathbf{d}_h$ and $\mathbf{d}_v$ such that $\mathbf{d}_h = \mathbf{W}_h\mathbf{D}_h\mathbf{x}_p$ and $\mathbf{d}_v = \mathbf{W}_v\mathbf{D}_v\mathbf{x}_p$. This reformulates the problem as,

$$(\hat{\mathbf{x}}_p, \hat{\mathbf{d}}_h, \hat{\mathbf{d}}_v) = \underset{\mathbf{x}_p,\mathbf{d}_h,\mathbf{d}_v}{\operatorname{argmin}} \tfrac{1}{2}||\mathbf{y}_p - \mathbf{A}\mathbf{x}_p||^2_{\mathbf{W}_{yp}} + \tau_p||\mathbf{d}_h||_1 + \tau_p||\mathbf{d}_v||_1 + \tfrac{\lambda_p}{2}||\mathbf{d}_h - \mathbf{W}_h\mathbf{D}_h\mathbf{x}_p||^2_2 + \tfrac{\lambda_p}{2}||\mathbf{d}_v - \mathbf{W}_v\mathbf{D}_v\mathbf{x}_p||^2_2 \quad (18)$$

where λ_p is the penalty parameter. Using simplified Bregman iterative scheme, the iterations are reformulated as,

$$\mathbf{x}_p{}^{k+1} = \underset{\mathbf{x}_p}{\operatorname{argmin}} \tfrac{1}{2}||\mathbf{y}_p - \mathbf{A}\mathbf{x}_p||^2_{\mathbf{W}_{yp}} + \tfrac{\lambda_p}{2}||\mathbf{d}_h^k - \mathbf{W}_h\mathbf{D}_h\mathbf{x}_p - \mathbf{b}_h^k||^2_2 + \tfrac{\lambda_p}{2}||\mathbf{d}_v^k - \mathbf{W}_v\mathbf{D}_v\mathbf{x}_p - \mathbf{b}_v^k||^2_2 \quad (19)$$

$$\mathbf{d}_h{}^{k+1} = \underset{\mathbf{d}_h}{\operatorname{argmin}} \tau_p||\mathbf{d}_h||_1 + \frac{\lambda_p}{2}||\mathbf{d}_h - \mathbf{W}_h\mathbf{D}_h\mathbf{x}_p^{k+1} - \mathbf{b}_h^k||^2_2 \quad (20)$$

$$\mathbf{d}_v{}^{k+1} = \underset{\mathbf{d}_v}{\operatorname{argmin}} \tau_p||\mathbf{d}_v||_1 + \frac{\lambda_p}{2}||\mathbf{d}_v - \mathbf{W}_v\mathbf{D}_v\mathbf{x}_p^{k+1} - \mathbf{b}_v^k||^2_2 \quad (21)$$

$$\mathbf{b}_h{}^{k+1} = \mathbf{b}_h^k + (\mathbf{W}_h\mathbf{D}_h\mathbf{x}_p^{k+1} - \mathbf{d}_h^{k+1}) \quad (22)$$

$$\mathbf{b}_v{}^{k+1} = \mathbf{b}_v^k + (\mathbf{W}_v\mathbf{D}_v\mathbf{x}_p^{k+1} - \mathbf{d}_v^{k+1}) \quad (23)$$

Equation (19) has a closed form solution as,

$$\mathbf{x}_p{}^{k+1} = (\mathbf{A}^T\mathbf{W}_{yp}\mathbf{A} + \lambda_p\mathbf{D}_h^T\mathbf{W}_h^T\mathbf{W}_h\mathbf{D}_h + \lambda_p\mathbf{D}_v^T\mathbf{W}_v^T\mathbf{W}_v\mathbf{D}_v)^{-1} (\mathbf{A}^T\mathbf{W}_{yp}\mathbf{y}_p + \lambda_p\mathbf{D}_h^T\mathbf{W}_h^T(\mathbf{d}_h^k - \mathbf{b}_h^k) + \lambda_p\mathbf{D}_v^T\mathbf{W}_v^T(\mathbf{d}_v^k - \mathbf{b}_v^k)) \quad (24)$$

and equations (20) and (21) can be found via shrinkage operations as,

$$\mathbf{d}_h{}^{k+1} = shrink(\mathbf{W}_h\mathbf{D}_h\mathbf{x}_p{}^{k+1} + \mathbf{b}_h^k, \frac{\tau_p}{\lambda_p}) \quad (25)$$

$$\mathbf{d}_v{}^{k+1} = shrink(\mathbf{W}_v\mathbf{D}_v\mathbf{x}_p{}^{k+1} + \mathbf{b}_v^k, \frac{\tau_p}{\lambda_p}) \quad (26)$$

with

$$shrink(u, w) = sgn(u) * \max(|u| - w, 0) \quad (27)$$

Experiments and Results

In this section we present results from experimental data acquired from the Imatron C300 electron-beam medical scanner. For our experiments we used 95 kVp and 130 kVp spectra (kVp denotes the maximum voltage applied to the X-ray tube). Estimates of the energy spectra are shown in Fig. 1. The re-binned parallel sinograms have 720 angles and 1024 detector bins. Reconstructions of two slices from a bag which contained a water bottle, a rubber sheet and various degrees of metal clutter are presented. The reconstructed images are 512x512 with a pixel spacing of 0.928 mm.

Fig. 2 shows the initial reconstructions of the high-energy images of slice 1 and slice 2. These are reconstructed by minimizing weighted least squares with TV regularization as explained in (13). Fig. 3 shows the low-energy sinogram and the corresponding condition numbers of the covariance matrices of the estimated basis sinograms of slice 1. The bright rays of the sinogram are the rays that pass through metal and as can be seen the condition numbers follow a similar pattern.

For the reconstructions, in order to construct the forward projection matrix we have utilized the ASTRA toolbox [13], specifically the spot-operator called *opTomo*. The toolbox uses CUDA for NVIDIA GPUs to perform accelerated parallel computations. To update the coefficients in each iteration, (sub-problem 19) we used *Matlab* inbuilt generalized minimum residual method (GMRES).

Reconstruction Results

Fig. 4 shows reconstruction results of Compton and photoelectric images for the two slices reconstructed with filtered backprojection (FBP), minimizing least squares with TV regularization (LS with TV), minimizing weighted least squares with TV regularization (WLS with TV), proposed method, and SPDE inversion method. Note that the coefficients are for when using normalized basis functions.

Figs. 4a, 4b, 4c and 4d are the results from FBP. Both the Compton and the photoelectric images have streaks caused by metal scatter, but the photoelectric images are highly distorted and the underlying structures can be barely made out.

Figs. 4e, 4f, 4g and 4h are the reconstruction results of minimizing least squares with TV regularization. Here the noise artifacts have reduced in all images, but the metal induced streaks are still visible. For these reconstructions the regularization parameters were chosen as $\tau_c = 100$, $\beta_c = 5000$, $\tau_p = 2000$ and $\beta_c = 50000$. Note that for Compton images we can increase regularization to obtain over-smoothed images with less streaks but the underlying structure will not be preserved. The photoelectric images are still highly corrupted and even with high regularization the images cannot be corrected.

Figs. 4i, 4j, 4k and 4l are the reconstruction results of minimizing weighted least squares with TV regularization. Here weights were calculated using inverse of covariance matrices as described earlier. As seen, down-weighting the Compton sinogram has introduced additional distortions in Fig. 4i in the region of the rubber sheet. As discussed earlier we believe this is due to the nearly singular covariance matrices of the highly clustered corrupted projection rays. However, down-weighting the photoelectric sinogram have significantly reduced the metal streaks.

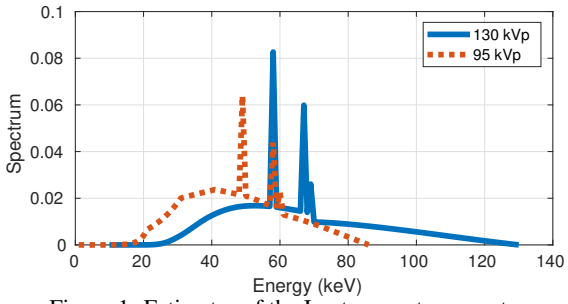

Figure 1: Estimates of the Imatron system spectra

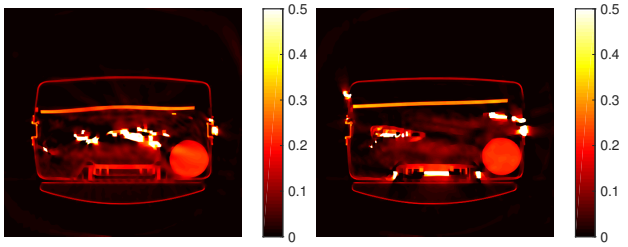

(a) (b)

Figure 2: Initial reconstructions of the high-energy images of (a) slice 1, (b) slice 2.

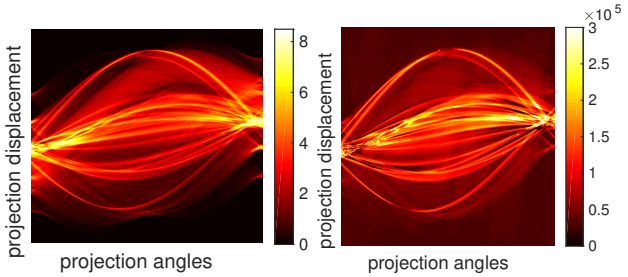

(a) (b)

Figure 3: (a) Low-energy sinogram, (b) corresponding condition numbers of the covariance matrices of the estimated decomposed sinograms, of slice 1. The condition numbers are higher for rays passing through metal.

Now the underlying structures can slightly be made out in Figs. 4j and 4l, but the images are clearly over-smoothed. The regularization parameters chosen for this case were $\tau_c = 10$, $\beta_c = 500$, $\tau_p = 2000$ and $\beta_c = 50000$.

Figs. 4m, 4n, 4o and 4p are the reconstruction results from the proposed EPTV regularization method. The Compton sinograms are not weighted, while the photoelectric sinograms are weighted. The metal induced streaks have clearly reduced in all of the images. The Compton images have preserved the underlying structure, and the edges are much sharper when comparing with reconstruction of just using TV regularization. The photoelectric images have also preserved a significant amount of the structure. The regularization parameters chosen were $\tau_c = 500$, $\beta_c = 12000$, $\tau_p = 2000$ and $\beta_c = 50000$. Note that the optimal regularization parameters were empirically chosen for all of the algorithms described above.

Finally we compare the reconstructions with results from SPDE inversion method [8] in Figs. 4q, 4r, 4s and 4t. Note that instead of the weights proposed in the paper, here we use the inverse covariance as weights and we only down-weight the photoelectric sinogram to make the method comparable with the proposed method. Even though the results are favorable they do not preserve the structure as well as the proposed method.

Quantitative Results

To provide quantitative results of image improvements we manually segmented the homogeneous areas of rubber and water (excluding boundaries) and calculated the signal to noise ratio (SNR) of the Compton and photoelectric coefficients, where SNR was defined as the mean divided by the standard deviation. Fig. 5 shows the SNR values obtained for water and rubber segmentations in both slices.

For the reconstructions from FBP and minimizing least squares with TV regularization, the obtained SNR values are much lower, specially for photoelectric coefficients. For the reconstructions from minimizing weighted least squares with TV regularization and SPDE, good SNR values have been obtained in the water region, but the SNR values in the rubber region are low. However, when using the proposed method with EPTV regularization, higher SNR values have been obtained in both water and rubber regions for both Compton and photoelectric coefficients.

The whole reconstruction process (starting with dual-energy measurements and reconstructing Compton and photoelectric images) with the proposed method took on average 193.5 secs per slice with the current implementation on *Matlab*. Even though it is much more computationally intensive than FBP, it is comparable with other model-based iterative methods. In comparison, the SPDE inversion took 211 secs per slice on average.

Discussion

In this paper, we presented a novel algorithm to reduce the noise and metal artifacts in dual-energy CT images. The algorithm was based on minimizing weighted least squares with edge-preserving total variation regularization. We exploited the mutual structure between the Compton and photoelectric images. Furthermore to correct metal artifacts in photoelectric images, we applied explicit data weighting to the photoelectric sinogram.

Using experimental data, we compared the proposed algorithm with alternative methods. Qualitative reconstruction results indicated that the proposed method is capable of removing noise and metal artifacts, and preserving the underlying structure simultaneously. Other iterative methods have a trade-off between these two features. Furthermore we showed that the proposed method is capable of obtaining high SNR values for all regions. We also verified that the reconstruction time for the proposed method is in the same order of magnitude with the other iterative methods.

Hence, the proposed algorithm shows promise as an alternative inversion technique for dual-energy images, which would lead to increase accuracy in material identification.

The main limitation of our algorithm is the computational complexity. The bottleneck lies in the sub-problem (19) which cannot be parallelized since the entire image needs to be updated per each inner-iteration of GMRES or any other similar solver. In future, we are looking into how to structure the computations such that we can exploit parallelism. Furthermore we believe it will be worthwhile to combine single-energy sinogram-based metal artifact reduction techniques with the proposed dual-energy reconstruction algorithm to obtain better results.

References

[1] A. Kak and M. Slaney, Principles of computerized tomographic imaging, IEEE press (1988).

[2] R.E. Alvarez and A. Macovski, Energy-selective reconstructions in X-ray computerised tomography, Physics in Medicine & Biology, V.21, No.5 (1976).

[3] S. G. Azevedo, H. E. Martz, M. B. Aufderheide, W. D. Brown, K. M. Champley, J. S. Kallman, G. P. Roberson, D. Schneberk, I.M. Seetho, and J. A. Smith, System-independent characterization of ma-

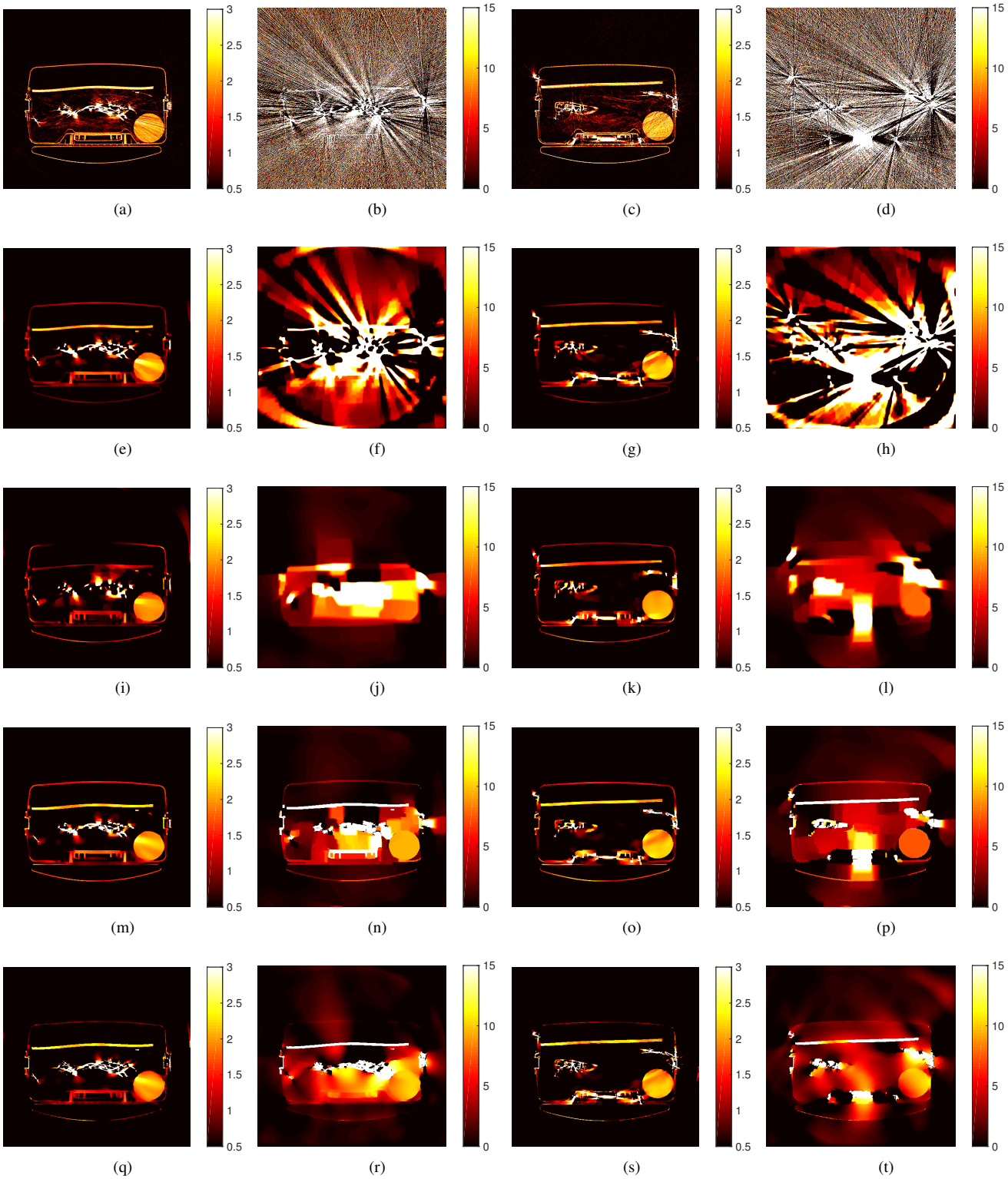

Figure 4: Compton images (columns 1 & 3) and photoelectric images (columns 2 & 4) of slice 1 (left two columns) and slice 2 (right two columns). Results from, top row : FBP, 2^{nd} row: LS with TV, 3^{rd} row: WLS with TV , 4^{th} row: proposed method, 5^{th} row: SPDE.

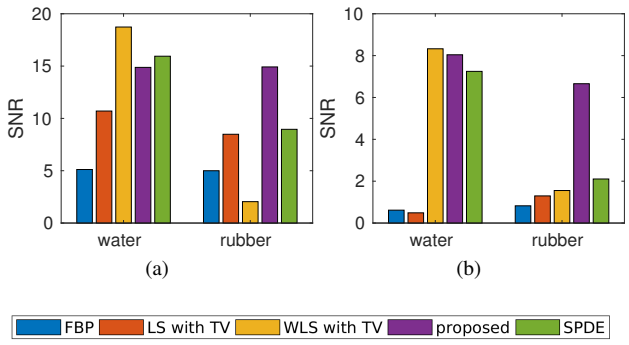

Figure 5: SNR of: (a) Compton image, (b) photoelectric image

terials using dual-energy computed tomography, IEEE Transactions on Nuclear Science, V.63, No.1 (2016).

[4] Z. Ying, R. Naidu, and C. R. Crawford, Dual energy computed tomography for explosive detection, Journal of X-ray Science and Technology, V.14, No.4 (2006).

[5] L. Gjesteby, B. De Man, Y. Jin, H. Paganetti, J. Verburg, D. Giantsoudi, and G. Wang, Metal artifact reduction in CT: where are we after four decades?, IEEE Access, V.4 (2016).

[6] P. Babaheidarian, and D. Castañón, A randomized approach to reduce metal artifacts in X-Ray computed tomography, IS &T International Symposium on Electronic Imaging : Computational Imaging XV (2017).

[7] B. H. Tracey and E. L. Miller, Stabilizing dual-energy X-ray computed tomography reconstructions using patch-based regularization, Inverse Problems, V.31, No.10 (2015).

[8] L. Martin, W.C. Karl, and P. Ishwar, Structure-preserving dual-energy CT for luggage screening, IEEE International Conference on Acoustics, Speech and Signal Processing (2014).

[9] Z. Tian, X. Jia, K. Yuan, T. Pan, and S. B. Jiang, Low-dose CT reconstruction via edge-preserving total variation regularization, Physics in Medicine & Biology, V.56, No.18, (2011).

[10] T. Goldstein and S. Osher, The split-Bregman method for L1-regularized problems, SIAM Journal on Imaging Sciences, V. 2, No 2 (2009).

[11] K. Sauer, and C.Bouman, A local update strategy for iterative reconstruction from projections, IEEE Transactions on Signal Processing, V.41, No.2 (1993).

[12] J. Nocedal and S. J. Wright, Numerical Optimization, Springer Series in Operations Research. Springer (1999).

[13] W. van Aarle, W.J. Palenstijn, J.Cant, E.Janssens, F. Bleichrodt, A. Dabravolski, J.De Beenhouwer, K.J. Batenburg and J.Sijbers, Fast and flexible X-ray tomography using the ASTRA toolbox, Optics Express, V.24, No.22 (2016).

Author Biography

Sandamali Devadithya received the B.Sc. degree (Hons.) in electronics and telecommunication engineering from the University of Moratuwa, Sri Lanka, in 2013, and the M.S.E.E. degree from the University of Washington, Seattle, USA, in 2017. She is currently a Ph.D. candidate at the Department of Electrical and Computer Engineering, Boston University, Boston, USA. Her current research interests include digital signal processing, inverse problems, computational imaging and sensing.

David Castañón is Professor of Electrical and Computer Engineering at Boston University. He received his Ph.D. in applied mathematics from MIT (1976). He was Chief Scientist at ALPHATECH before joining Boston University (1990). He has been ECE Department Chair, co-director of the Center for Information and Systems Engineering, President of the IEEE Control Systems Society, and member of Air Forces Scientific Advisory Board. His interests include control, estimation, optimization,inverse problems and image understanding.

JOIN US AT THE NEXT EI!

IS&T International Symposium on

Electronic Imaging

SCIENCE AND TECHNOLOGY

Imaging across applications . . . Where industry and academia meet!

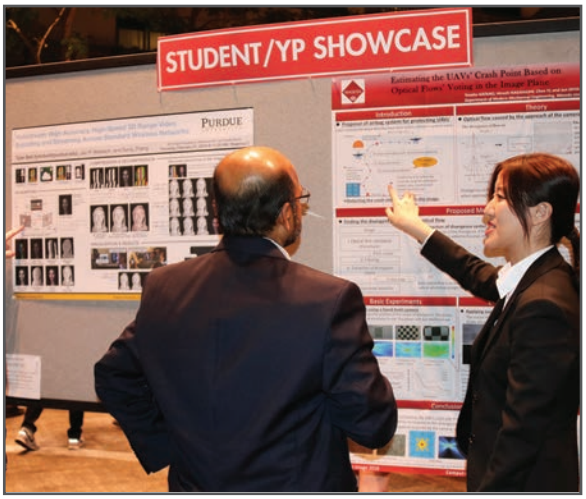

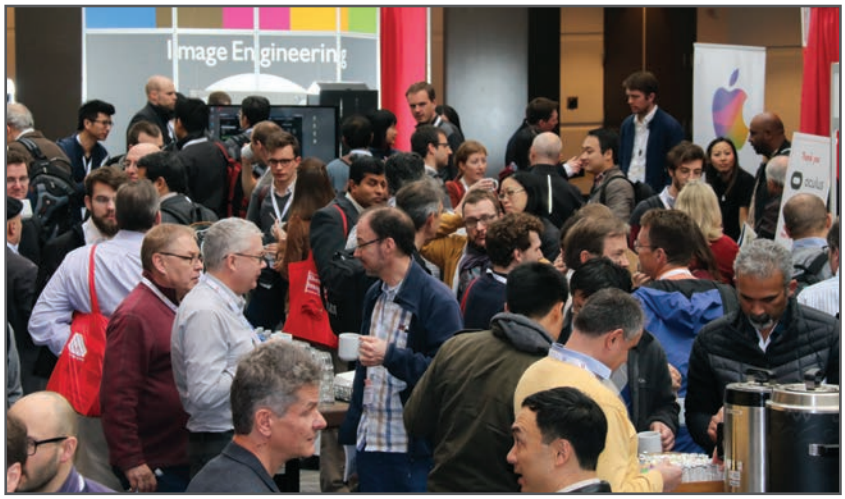

• SHORT COURSES • EXHIBITS • DEMONSTRATION SESSION • PLENARY TALKS •
• INTERACTIVE PAPER SESSION • SPECIAL EVENTS • TECHNICAL SESSIONS •

www.electronicimaging.org

IS&T
imaging.org